Materials Characterization 100 (2015) 1–12

Contents lists available at ScienceDirect

Materials Characterization

journal homepage: www.elsevier.com/locate/matchar

Tutorial review

The TriBeam system: Femtosecond laser ablation in situ SEM

McLean P. Echlin [a,*], Marcus Straw [b], Steven Randolph [b], Jorge Filevich [b], Tresa M. Pollock [a]

[a] Materials Department, University of California — Santa Barbara, Santa Barbara, CA 93106-5050, USA
[b] FEI Company, 5350 NE Dawson Creek Drive, Hillsboro, OR 97124, USA

ARTICLE INFO

Article history:
Received 17 July 2014
Received in revised form 20 October 2014
Accepted 25 October 2014
Available online 30 October 2014

Keywords:
Femtosecond laser
Tomography
Ablation
Serial sectioning
Ultrafast laser chemistry

ABSTRACT

Femtosecond laser ablation offers the unique ability to remove material at rates that are orders of magnitude faster than existing ion beam technologies with little or no associated damage. By combining ultrafast lasers with state-of-the-art electron microscopy equipment, we have developed a TriBeam system capable of targeted, in-situ tomography providing chemical, structural, and topographical information in three dimensions of near mm^3 sized volumes. The origins, development, physics, current uses, and future potential for the TriBeam system are described in this tutorial review.

1. Brief history of development

The development of ultrashort pulse lasers (UPL) in the mid-1980's by Strickland and Mourou [1] ushered in a host of advancements in technologies as wide ranging as spectroscopy, X-ray diffraction, micromachining, tissue modification, femtochemisty, and material processing [2–11]. While these new capabilities are applicable across a broad range of material classes (metals, ceramics, semiconductors, polymers, soft tissues, and composites), to date they have been applied mainly in ambient laboratory environments. Given the rapid, athermal, nm-scale material modification possible with ultrashort pulses, the in vacuo combination of UPL with electron and ion beams, and the micro-analytical techniques they enable, promises entirely new frontiers of material synthesis and characterization. Here we describe the motivation for and development of a new instrument that integrates a femtosecond laser with a scanning electron microscope (SEM) and a focused ion beam (FIB).

The historical development of the TriBeam traces a dual path. Early ex situ experiments by Pollock et al. were motivated by (1) the micromachining of high strength and multilayered materials with minimal damage, (2) the development of spectroscopy and X-ray probes to characterize local material states and, (3) layer-by-layer ablation for 3-D material tomography. The following studies were all conducted using chirp pulse amplified (CPA) titanium sapphire (Ti:Sapphire) femtosecond lasers with approximately 150 fs pulse width and 1000 Hz repetition rate. Transmission and scanning electron microscopy studies of single crystal Ni-based materials subjected to a variety of micromachining and ablation procedures [12,13] demonstrated remarkably low levels of material damage with little residual melting and limited dislocation injection. Multilayered metallic/ceramic systems and reactive multilayers [8,14,15] were also sectioned with minimal damage. Laser-induced breakdown spectroscopy (LIBS) using ultrashort pulses was shown to chemically characterize materials with much higher signal to noise ratios than LIBS performed with longer pulses and enabled depth profiling through multilayers containing thin "marker" layers [16–19]. Additionally, ultrashort pulse LIBS, with material removal depths as small as 60 nm, effectively approach "non-destructive" material characterization [16]. Using terahertz time domain reflectometry, subsurface damage in thermally grown oxide layers was also demonstrated [20]. At higher fluences, X-ray generation from a target sample in ambient conditions [21,22] permitted both radiography and diffraction analysis of a closely located probe sample. Finally, tomographic material characterization was demonstrated via layer-by-layer ablation and sequential imaging [23,24]. The experimental setup originally employed is shown schematically in Fig. 1 where the laser beamline is shown in parallel to the imaging beamline. UPL serial sectioning was achieved either by scanning the sample beneath the stationary laser beam via stage movements or by using galvometric mirrors to raster the beam across the stationary sample. Between each ablated layer, a stage translation positioned the sample beneath the imaging beamline. Ultimately, the limitations of optical imaging motivated the pursuit of a higher resolution approach, leading to the development of the TriBeam [25], shown schematically in Fig. 2.

Simultaneous to the work of Pollock et al., an independent study exploring the potential of UPLs for increasing the throughput of processes normally performed on focused ion beam (FIB) and DualBeam systems began at FEI Company's research facility in Hillsboro, Oregon. To provide an experimental platform for this effort, a prototype instrument

* Corresponding author.
E-mail address: mechlin@engineering.ucsb.edu (M.P. Echlin).

http://dx.doi.org/10.1016/j.matchar.2014.10.023
1044-5803/

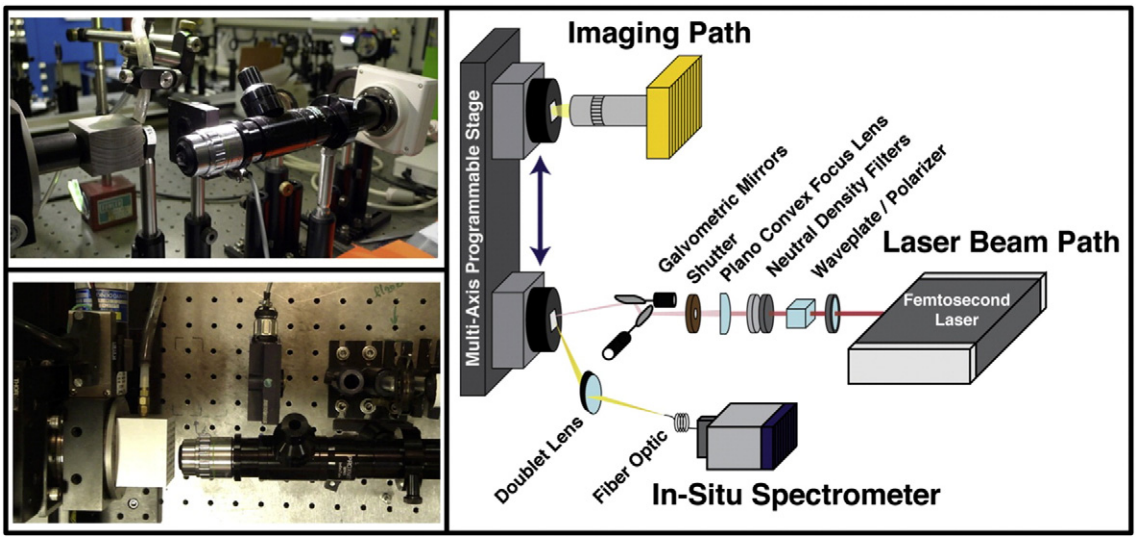

Fig. 1. A femtosecond laser based serial sectioning setup designed for use in open-atmosphere is shown schematically in the right with photos of the setup shown on the left [23]. This technique utilizes an optical microscope as the mode of imaging. The beam can be scanned on the sample surface either by using the multi-axis programmable translational stage, or by using galvometric mirrors. A spectrometer is also available for chemical analysis using the laser induced breakdown spectroscopy (LIBS) technique.

combining an FEI DualBeam and a chirped pulse amplification (CPA) titanium sapphire (Ti:Sapphire) laser system was developed. The CPA lasers used were identical to those mentioned in the work of Pollock et al. While the primary applications targeted were those requiring the rapid removal of large volumes of material such as failure and defect analysis of semiconductor devices, depackaging of ICs, MEMS prototyping, and the characterization of porosity and connectivity in geological samples, the TriBeam was also applied to a variety of exploratory applications extending beyond material processing. For instance, in situ laser-based characterization techniques such as Raman spectroscopy and LIBS were explored as a means of generating correlative data. Demonstrating the instrument's efficacy for exploring the interaction of light and matter, electron beam-induced deposition (EBID) templated UPL-mediated surface chemistry was explored as a means of rapidly depositing micro- and nano-structures [26]. Similarly, ex situ studies demonstrated the use of UPL-induced plasma mediated chemical reactions to volatilize ablated material, effectively mitigating contamination of the vacuum [27].

Having complementary goals, these two independent research groups ultimately joined efforts to form a collaboration. Early in the collaboration, a detailed review of the prototype TriBeam system led to a second version of the instrument incorporating component improvements designed by Pollock et al. In particular, an improved laser injection port (LIP) design along with the incorporation of a fast steering mirror and a piezo sub-stage resulted in a more robust and flexible instrument ideally suited for tomography [25]. The third and most recent version enclosed the beam line and added automated beam stabilization. Presently, the TriBeam instrument consists of a femtosecond laser combined with an FEI Quanta 3D FEG DualBeam system (FIB-SEM). The multiple imaging modalities of the DualBeam – including electron backscatter diffraction (EBSD), energy dispersive X-ray spectroscopy (EDS), and backscatter (BSE) and secondary electron (SE) detection – enable the analysis of a sample's crystalline structure, chemical composition, relative atomic mass, and surface topography respectively.

2. Light-matter interactions on the femtosecond time scale

Ultrashort pulses are those having a duration between 1 fs and 10 ps. Functionally, “ultrashort” describes the regime entered when the material response to an incident pulse is non-linear, i.e. when it is dominated by the square (or higher order) terms of the

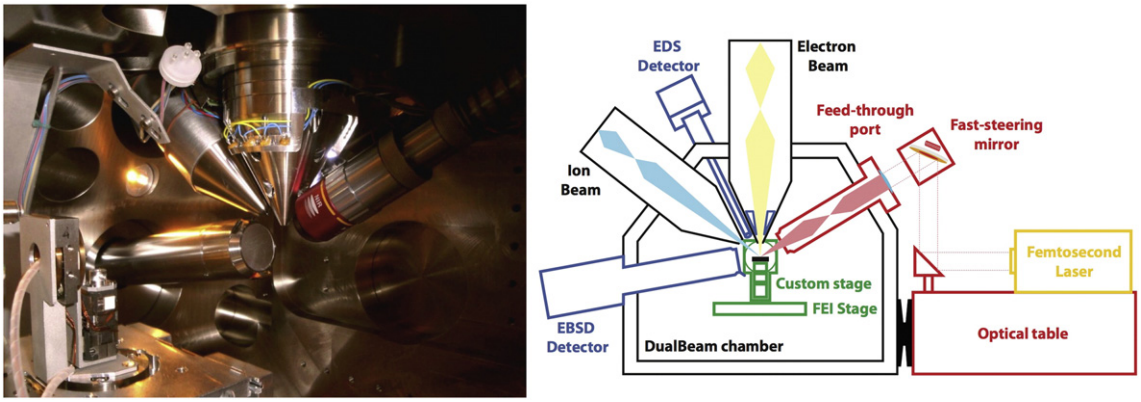

Fig. 2. (Left) An image of the inside of vacuum chamber is shown with the EBSD camera inserted and the stage door open. (Right) Schematic of the TriBeam system with Ga+ source ion beam, femtosecond laser, electron beam, and EBSD and EDS detectors. The custom piezo stages are mounted on top of the existing microscope stages. The setup is shown in more detail in [25].

electric field. As an example, consider the polynomial expansion of the macroscopic polarization P of a material illuminated by laser pulse having an electric field E:

$$\frac{\mathbf{P}}{\epsilon_0} = \chi^{(1)} \cdot \mathbf{E} + \chi^{(2)} \cdot \mathbf{EE} + \chi^{(3)} \cdot \mathbf{EEE} + \ldots \quad (1)$$

where ϵ_0 is the vacuum permittivity and $\chi^{(n)}$ is the *nth* order of the electric susceptibility. The second and higher order terms describe the non-linear response of the polarization. When laser pulses are shorter than about 10 ps, the electric field is large enough that the higher order terms in Eq. (1) grow larger than the first order term in spite of the large difference in the susceptibility terms, effectively inducing non-linear effects in the material.

Ultrashort pulses can achieve very high peak powers at relatively small pulse energies, when focused to spot sizes with areas of a few square microns. In fact, ultrashort pulses reach power density orders of magnitude greater than the power density of the sun's photosphere. At these extreme intensities, non-linear effects dominate and light is absorbed through mechanisms such as multi-photon absorption [28–30]. At sufficiently high laser intensities, the photon flux and thus the electric field can exceed that required to create a solid density plasma in the target. The resulting free electrons diffuse through the material or escape the bulk altogether as photoelectrons. The remaining ions can repel one another explosively in a process typically referred to as coulombic explosion [29]. The resulting material removal event, accompanied by the formation and expansion of a plasma plume, is commonly referred to as ablation.

Ultrashort pulses interact with matter on a timescale that is dramatically shorter than the physical processes they drive. The timescales of an ablation event is shown in Fig. 3. Models show that in metals, electron excitation occurs within the first 150 fs in the top 10's of nm of the sample, with material response beginning tens to hundreds of picoseconds later [31,32]. Long after the pulse is off, between 0.2 and 1 ns, the irradiated material volumetrically expands and ejects from the sample surface via nucleation and cavitation [33]. Defects such as vacancies, self interstitials, and Frenkel pairs are stabilized at these short timescales by hydrostatic stresses that occur in shock loading conditions that provide the nucleation sites for cavitation [34,35]. The velocity of the ablatants has been measured using femtosecond laser shadowgraphy and pump-probe methods [36–38], which use a femtosecond pulse as the illumination probe, thereby improving the temporal resolution of the experiment to the pulse width of the beam. These experiments indicate that material is ejected from the surface at average velocities between 5,000 and 10,000 m/s with a shockwave propagating in air at roughly twice that speed [39]. The timescales at which the processes contributing to ablation occur result in a special set of conditions such as a small heat affected zone [40], and low collateral dislocation damage [12,41]. The specifics of the light-material interactions will be discussed in terms of material removal and surface modification in the following sections.

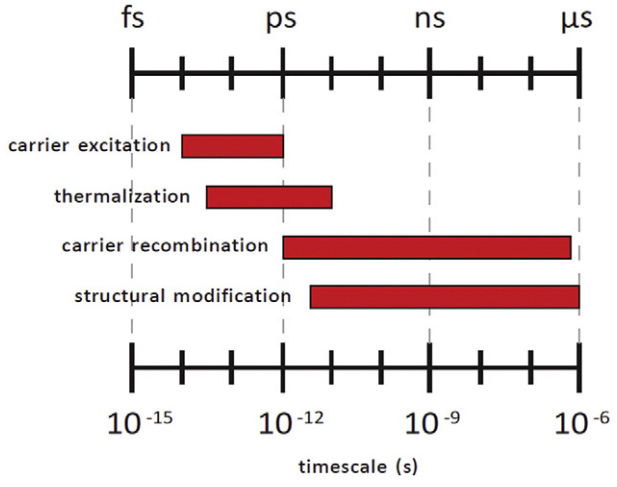

Fig. 3. Ultrashort pulse laser ablation is a complex multi-step process involving the following: (i) carrier excitation via multi-photon absorption, single photon absorption, Zener tunneling, free carrier absorption (metals), and/or avalanche ionization; (ii) thermalization due to carrier–carrier and carrier–phonon scattering; (iii) carrier depletion via radiative, Auger, defect, and surface recombination, and diffusion; and (iv) structural modification due to ablation, melting, thermal diffusion, and resolidification [91].

2.1. Removal rates

Commercial femtosecond lasers employing Ti:Sapphire gain mediums have relatively high pulse energies (>0.1 mJ/pulse) and can operate at repetition rates of 1–5 kHz. The beam from these laser systems can be focused with conventional optics to spot sizes from hundreds of microns down to the diffraction limit of the beam and easily achieve focused intensities high enough to ablate most solids independent of their optical properties. The flexibility of spot size and repetition rate enable the removal of material on a range of length scales from millimeters to tens of nanometers.

The minimum depth of removal (discussed in Section 2.2) is bounded by the low-fluence ablation threshold rate, which is typically 30–50 nm/pulse for most materials. Larger volumes can be removed by scanning the beam, routinely ablating regions that are 1 mm × 1 mm with depths between 0.1 and 100 µm. At typical laser operating fluences (1–40 J/cm^2), rates of 4×10^4 µm^3/s are routinely achieved, which is 4–5 orders of magnitude faster than a modern 65 nA Ga^+ ion beam [25,23], and 2–3 orders of magnitude faster than a plasma FIB [42,43].

2.2. Ablation thresholds

Femtosecond laser damage is a material response characterized by a set of sharp thresholds, one for the onset of ablation [44,45,13] and a second high fluence threshold at which there is an abrupt increase in material removal rate. Fig. 4 illustrates this principle with ablation threshold data for a high strength steel alloy having an ablation

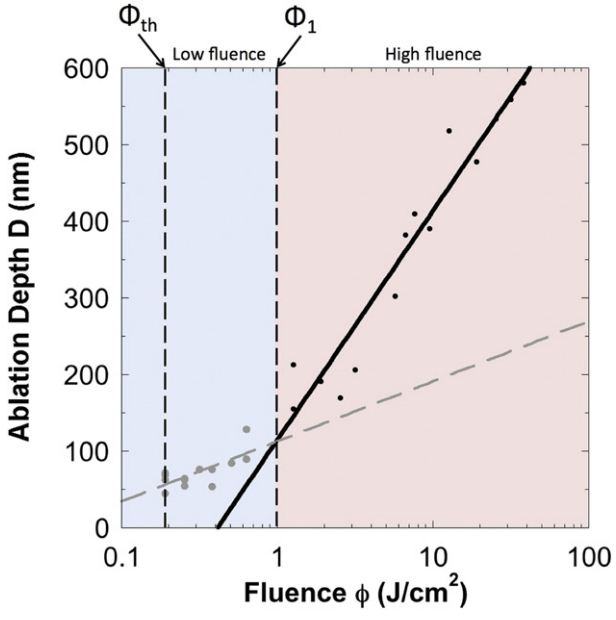

Fig. 4. This plot shows single pulse ablation depths, the ablation threshold ϕ_{th}, and the low fluence to high fluence transition ϕ_1 measured for a 4330 high strength steel. Fluences between 0.2 J/cm^2 and 1 J/cm^2 are considered to be in the low fluence regime. Above 1 J/cm^2 a distinct change in slope occurs, which is indicative of transition to the high fluency regime. Depth measurements were made using an AFM in tapping mode. More details about the experiment can be found elsewhere [92].

threshold ϕ_{th} and a low/high fluence transition ϕ_1 as indicated on the chart. The fluence range between ϕ_{th} and ϕ_1 is called the low fluence regime, which is typically characterized by a small heat affected zone (HAZ) and low amounts of dislocation injection. Fluences above ϕ_1 are described as the high fluence regime and can produce higher density dislocation injection and may also result in surface melting and resolidification. Note that ϕ_{th} and the ϕ_1 are both material properties.

2.3. Femtosecond laser ablation for micromachining

Laser-induced structuring can be controlled by (1) modifying the laser beam intensity or polarization and (2) changing the geometrical relation between the femtosecond beam and the sample. Consider a micromachining scheme in which the laser beam strikes the sample at a grazing angle and the beam is scanned parallel to the surface as

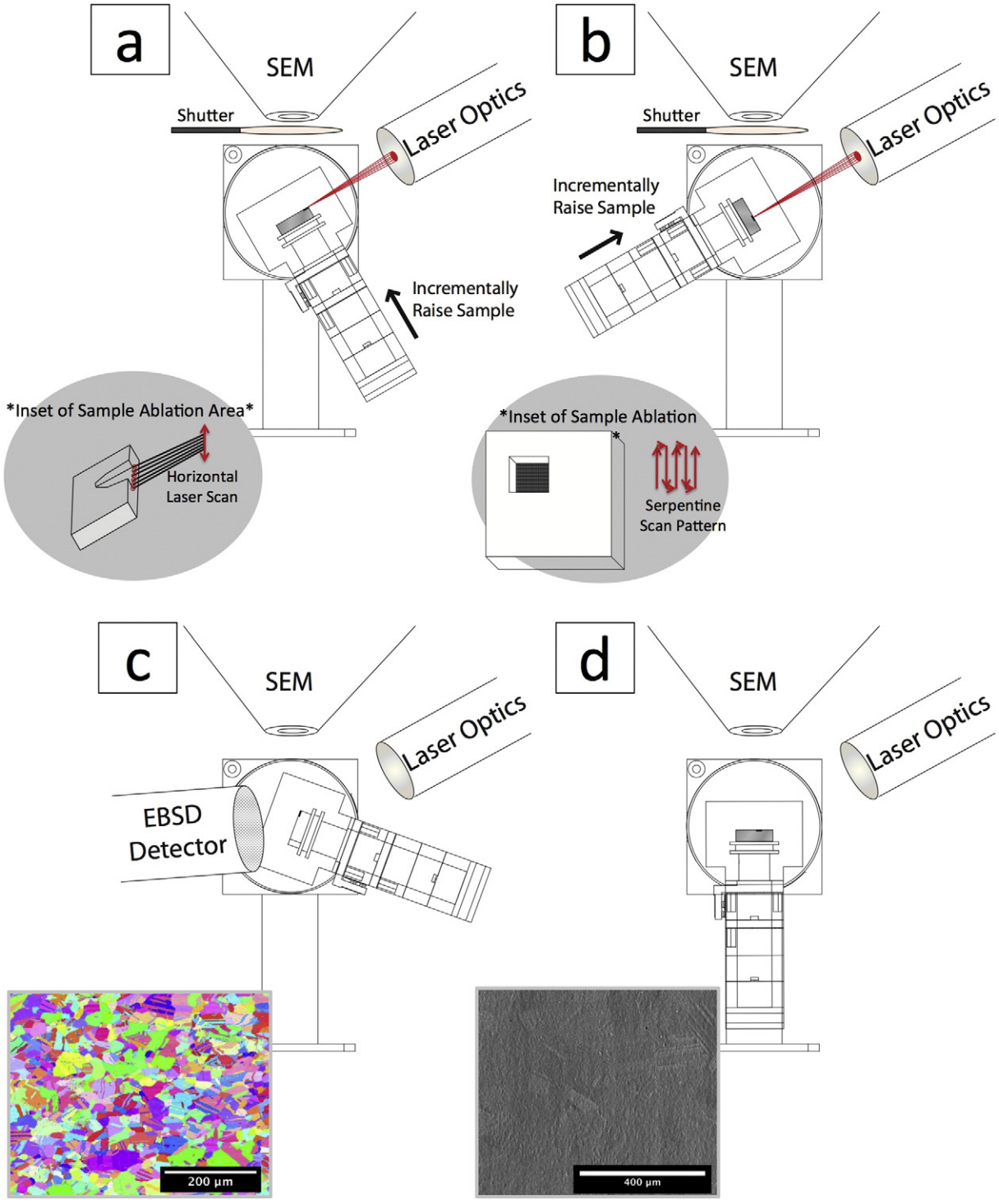

Fig. 5. A high-resolution piezo stage is used to position the sample between different detectors and beams within the SEM/FIB chamber. The laser beam is scanned with the sample surface parallel (a) or normal (b) to the beam. The setup in (a) is typically used for serial sectioning experiments, with slices made by raising the z-stage to bring the sample surface incrementally into the laser beam. The inset beneath (a) and (b) shows the examples of how the beam is scanned on the sample surface. EBSD imaging is made with the sample surface tilted 70° to the electron beam, shown in (c). SEM (SE, BSE) imaging is performed with the sample surface normal to the electron beam, shown in (d), or at any other arbitrary angle.

shown in Fig. 5(a). After multiple scanning passes of the femtosecond laser beam with a Gaussian to the surface profile, the low fluence tail of the intensity distribution will remove the final layer of material. Thus, even at high laser fluences, the ultimate surface morphology achieved using this configuration is largely governed by the low fluence regime.

When micromachining is performed with the beam oriented such that it is normal to the sample surface, as shown in Fig. 5(b), the choice of laser fluence becomes critical. In order to produce uniform multi-phase material removal, the laser machining fluence must be selected such that the ablation rate of all the constituent phases are matched. For example, a two-phase structure with a hard TiN phase embedded within a softer matrix steel phase requires ablation rates to be matched [23,24] in order to prevent preferential etching. However, preferential etching can be intentionally performed using laser beam fluences that are sub-optimized for the removal of unwanted phases [46], to provide contrast and corrosion resistance [47], or for other applications such as maskless photolithography [48].

2.4. Laser-induced surface structures

While substrates micromachined with femtosecond lasers suffer fewer laser-induced artifacts and less concomitant damage to adjacent structures than those machined with nanosecond or continuous wave lasers, ultrashort pulses are known to induce parallel, ripple-like surface structures commonly referred to as laser-induced periodic surface structures (LIPSS). An example of LIPSS formed by ultrashort pulse irradiation of a silicon sample is shown in Fig. 6. A significant body of literature exists exploring the mechanisms that drive the formation of these artifacts [49–58]. Though the majority of this work focuses on the formation of wavelength and sub-wavelength scale oscillations formed via the removal or reordering of material at the substrate surface during short and ultrashort pulse laser irradiation, Brueck and Ehrlich observed similar structures during "UV laser photolysis of organometallic molecular gases near a substrate surface" [59]. Identical phenomena have been observed in experiments with femtosecond laser-induced deposition and are described in Section 3.3.

Most authors now attribute the formation of LIPSS to surface plasmons generated by, and interacting with, the incident laser radiation. Recall that plasmons are quanta of oscillations induced when free charge carriers in a plasma are driven by an oscillating electric field. In a conducting medium, plasma oscillations result in density waves of carriers called Langmuir waves. Thus, plasmons are the quasi particles resulting from the quantization of such plasma waves. In metals, the movement of loosely bound electrons relative to their associated ions can be driven by the electromagnetic field of incident light. As a result, the optical properties of metals are dictated by the response of surface plasmons to the field. The plasma frequency ω_p of a metal is given by

$$\omega_p^2 = \frac{Ne^2}{\epsilon_0 m} \tag{2}$$

where ϵ_0 is the relative permittivity of the free space and N is density of free electrons that have charge e and mass m. If the frequency of light incident on the surface of a metal is below the plasma frequency ω_p, then electrons will screen the incident field and the light will be reflected. If the frequency of the light is higher than ω_p, the electrons cannot respond quickly enough to screen the field and the light is transmitted. The plasma oscillations responsible for these effects are referred to as surface plasmons. Longitudinal oscillations known as bulk plasmons are also possible, but because the electric field of incident photons is transverse, bulk plasmons cannot be excited by light at normal incidence.

According to Huang et al. [58], surface plasmons are generated when an ultrashort pulse interacts with a sample surface. As with all interference phenomena, the principle of superposition applies, leading to regions of field enhancement due to constructive interference and regions of field cancelation due to destructive interference. Given a laser pulse of sufficient fluence, the interference pattern induces permanent ripples on the sample surface, resulting in the formation of LIPSS with orientation perpendicular to the polarization of the electric field. As a result, the choice of polarization direction has a direct impact on the cut quality produced by a given serial sectioning procedure. While it is better to eliminate LIPSS altogether if possible, experiments show that LIPSS that form side-to-side across the face of a slice produce lower surface roughness than those that form parallel to the laser beam. Rigorous models that predict the topology of these LIPSS patterns remain to be developed. Parallel oriented LIPSS also exacerbate an effect known as curtaining [60], which is a surface structure caused by inhomogeneities in the sample density or topography. A curtain may form when a heterogeneity temporarily blocks the laser beam, causing a gradient in material removal in the region of the sample that is shadowed from the laser light. Thus, it is desirable to use p polarization when performing serial sectioning procedures with the femtosecond lasers in which the beam strikes the sample at a grazing angle. Curtains can be minimized by sample tilting, rocking, or rotating [60,61] and platinum caps [62,63]. Once initiated, curtaining artifacts are exacerbated by subsequent machining because of beam channeling.

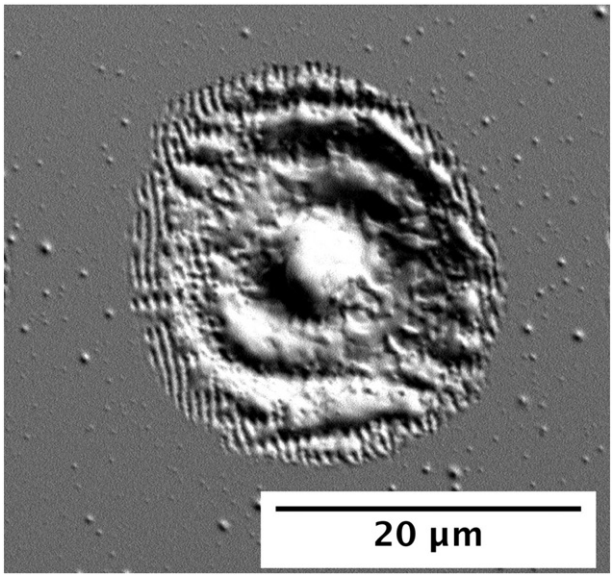

Fig. 6. A backscattered electron image (BSE) of laser-induced periodic surface structures (LIPSS) produced in silicon. The LIPSS are aligned vertically in the image with sub-micron periodicity.

2.5. Structural modification

Bulk laser machined specimens exhibit several different types of structural modification after ablation. These changes can be grouped into three categories: dislocation injection, recrystallization, and amorphization. As discussed in Section 2, the majority of the damage experienced by the sample is confined to the surface, which will be characterized presently.

Dislocation injection has been shown by TEM analysis for metals and ceramics in a number of different studies [13,12,64–67]. In most cases, there is a high density of dislocations immediately beneath the LIPSS structures, or in the lateral regions surrounding the area of ablation. The extent of the damage depends on the specific geometry of the pulse–sample interaction. In cases where the laser beam is normal to the surface (see Fig. 5(b)), the damage volume is governed by the Gaussian intensity distribution of the pulse. Ablation that occurs when the beam is oriented in this fashion can produce dislocation injection (estimated by grain misorientation) that scales with the peak fluence of the pulse. At very high laser fluences, dislocations have been observed at depths of up to 10 µm [41]. This dislocation damage can be mitigated by

tilting the sample until the beam is nearly parallel with the sample surface, shown in Fig. 5(a). Using this geometry, the damage profile characteristic of surface normal ablation is turned on its side. As a result, deep dislocations at the surface are removed via ablation and damage into the bulk is on the order of radial damage observed in low fluence ablation experiments [12]. In nickel alloys, the dislocations are confined to within hundreds of nanometers of the surface where LIPSS have formed, as shown in the FIB cross-section TEM images in Fig. 7.

2.5.1. Amorphization

In spite of its reputation as an athermal process, femtosecond laser ablation can amorphize crystalline samples under some conditions. The extent of the heat affected zone (HAZ) depends on the laser fluence, beam-sample geometry, and the material. FIB milling has been shown to produce amorphization in silicon with damage layers of 30 nm and 56 nm reported [68] for milling done with 30 kV beams at glancing angle and normal incidence, respectively. For comparison, TEM lamella were cross-sectioned from the sidewall of a silicon via that was machined with ultrashort pulses having fluence two orders of magnitude above the ablation threshold of silicon. As shown in Fig. 8, the HAZ (observed as amorphization) in the region analyzed, was measured to be approximately 20 nm. However, at laser fluences closer to the material ablation threshold, the amorphous region may be reduced even further.

Tungsten carbide has also been studied to determine the effect of femtosecond laser ablation on hard materials. WC-Co samples containing 11% cobalt with ≈10 μm grain size were femtosecond laser machined at parallel beam incidence to remove a volume of material of size 350 × 350 × 200 μm, a process that took approximately 10 min [26]. Afterward, lower fluence femtosecond laser polishing was performed on the surface. The images in Fig. 9(b and c) show the femtosecond laser machined surface in comparison to a mechanically polished WC-Co sample in Fig. 9(a). At higher magnifications, sub-wavelength periodic ripples are observed, shown in Fig. 9(c and d), similar to the LIPSS described in Section 2.4. TEM lamella were extracted, after depositing a protective platinum cap, from the laser machined cut face to analyze the crystallinity as a function of depth. Diffraction patterns were collected at varying distances from the laser ablated surface (shown in Fig. 10 (bottom)). The electron probe positions on the lamella are displayed as red crosses in Fig. 10 (top), for (left) bulk WC-Co, (middle) interface of bulk WC-Co/amorphous platinum cap region, and (right) amorphous platinum cap region. Comparison of the diffraction pattern collected in the bulk of the sample to the one collected at the bulk/Pt interface shows that the material at the interface is highly crystalline and that any heat deposited by the laser at the depth of the measurement was insufficient to melt or amorphize the sample.

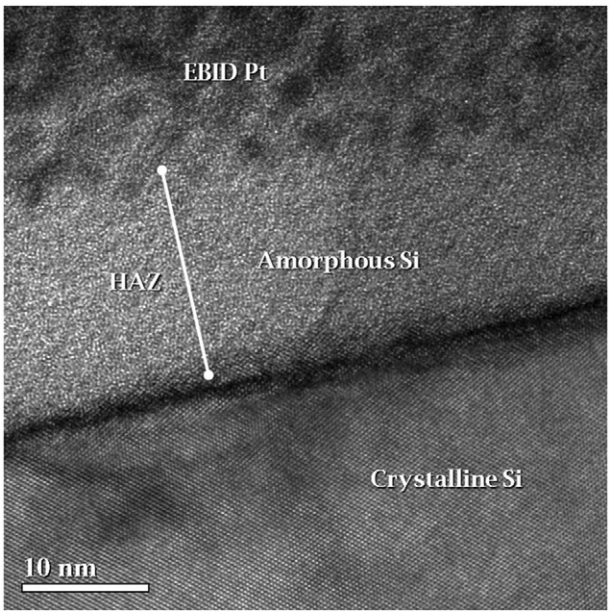

Fig. 8. Brightfield TEM images from a lamella that was cross-sectioned from a fs laser machined silicon sample at fluence 20x× the ablation threshold. The amorphization depth is ≈ 20 nm as indicated on the image.

3. TriBeam applications

Femtosecond lasers in FIB chambers have been primarily used for micromachining to date. Many other sub-ablation threshold applications that are routinely used in open-atmosphere have yet to be explored in situ though, such as laser induced breakdown spectroscopy [16–18, 69–71], and reflectivity studies [72,73]. In the following sections, the currently developed applications for in situ femtosecond laser will be discussed.

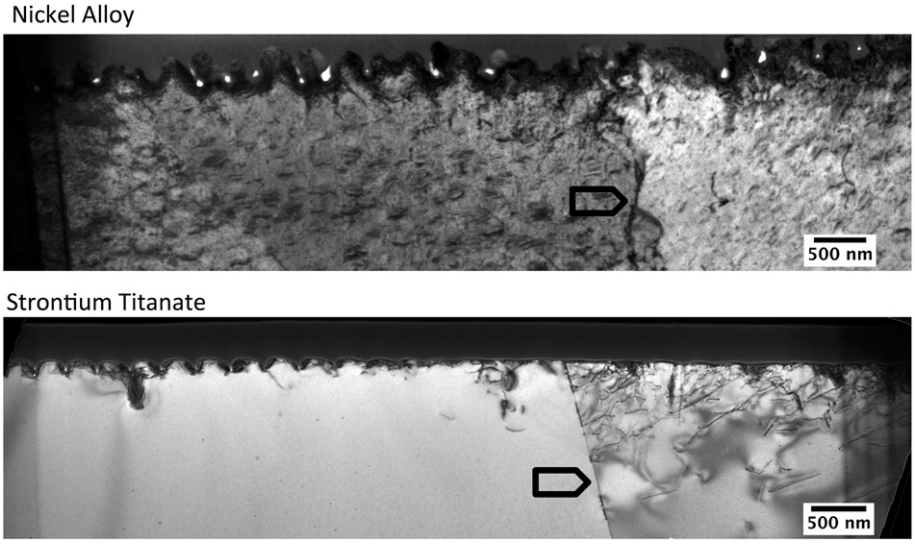

Fig. 7. Bright field TEM images of (top) a nickel alloy and (bottom) strontium titanate, that have both been laser machined by scanning the femtosecond laser beam parallel to the sample surface. Laser induced periodic structures (LIPSS) are visible in cross section on the surface of both samples. Grain boundaries are visible in both materials as indicated by arrows, with preferential dislocation injection depths apparent in the grain to the right in the STO material. The light gray contrast region at the top of each TEM micrograph, above the LIPSS, is a protective e-beam/i-beam deposited platinum cap.

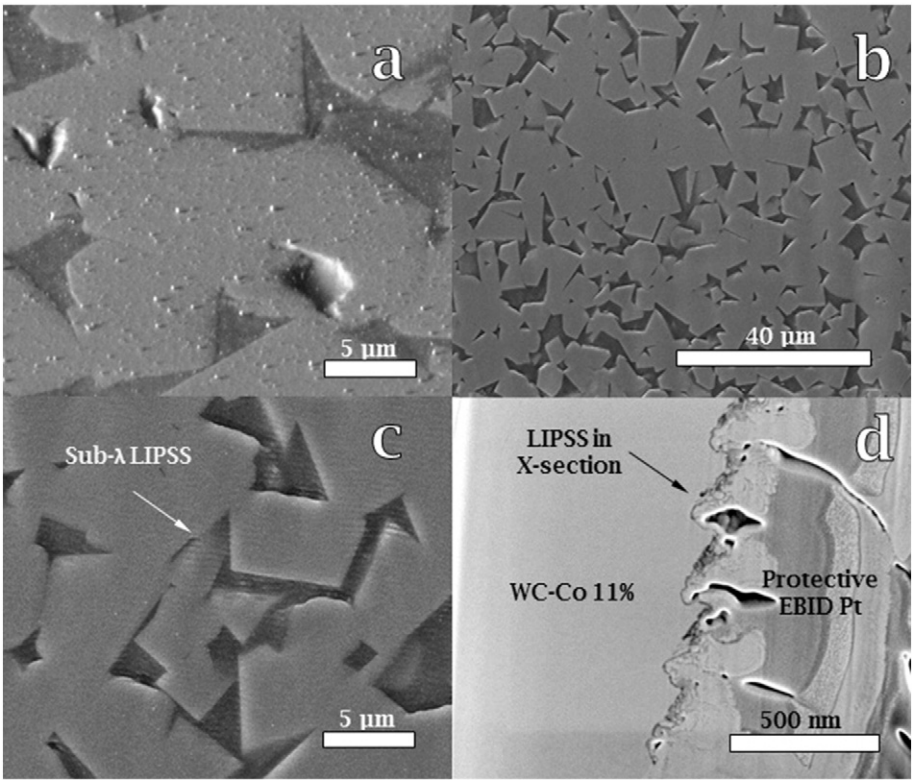

Fig. 9. Micrographs of a WC-Co sample. Figure Panel (a) shows a mechanically polished section of the sample, for comparison with (b,c) which show a laser machined surface at both low and high magnifications. Figure Panel (d) is a TEM image of the periodic surface structures, illustrating that the wavelength of the features is approximately 250 nm and have has an amplitude of 75-–100 nm.

3.1. 3D tomography

The acquisition of large 3D serial sectioning datasets using the TriBeam system requires substantially less time than existing destructive tomography systems and permits sectioning of complex engineering materials which may have multiple phases, a wide range of densities, and require multiple image modalities to characterize. The method for serial sectioning involves iterating between the following steps: (1) removing material using the scanned femtosecond laser beam and (2) imaging of the exposed surface and (3) performing additional chemical or crystallographic analysis of the surface. Laser machining for the removal of a controlled amount of material can be performed with the sample surface

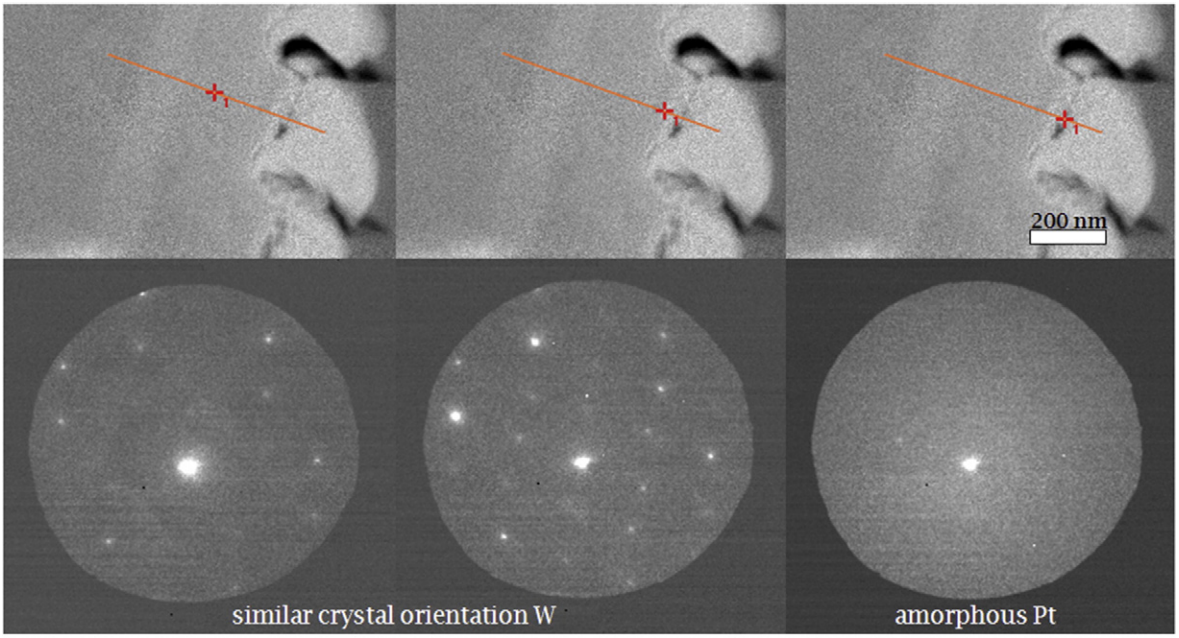

Fig. 10. Electron diffraction analysis of laser polished WC-Co. The location of the electron probe is indicated with red crosses on the upper images. No difference is apparent between the crystalline structure of the bulk (lower left hand diffraction pattern) and that of the material at the UPL polished interface (lower middle diffraction pattern), suggesting very little laser-induced thermal damage.

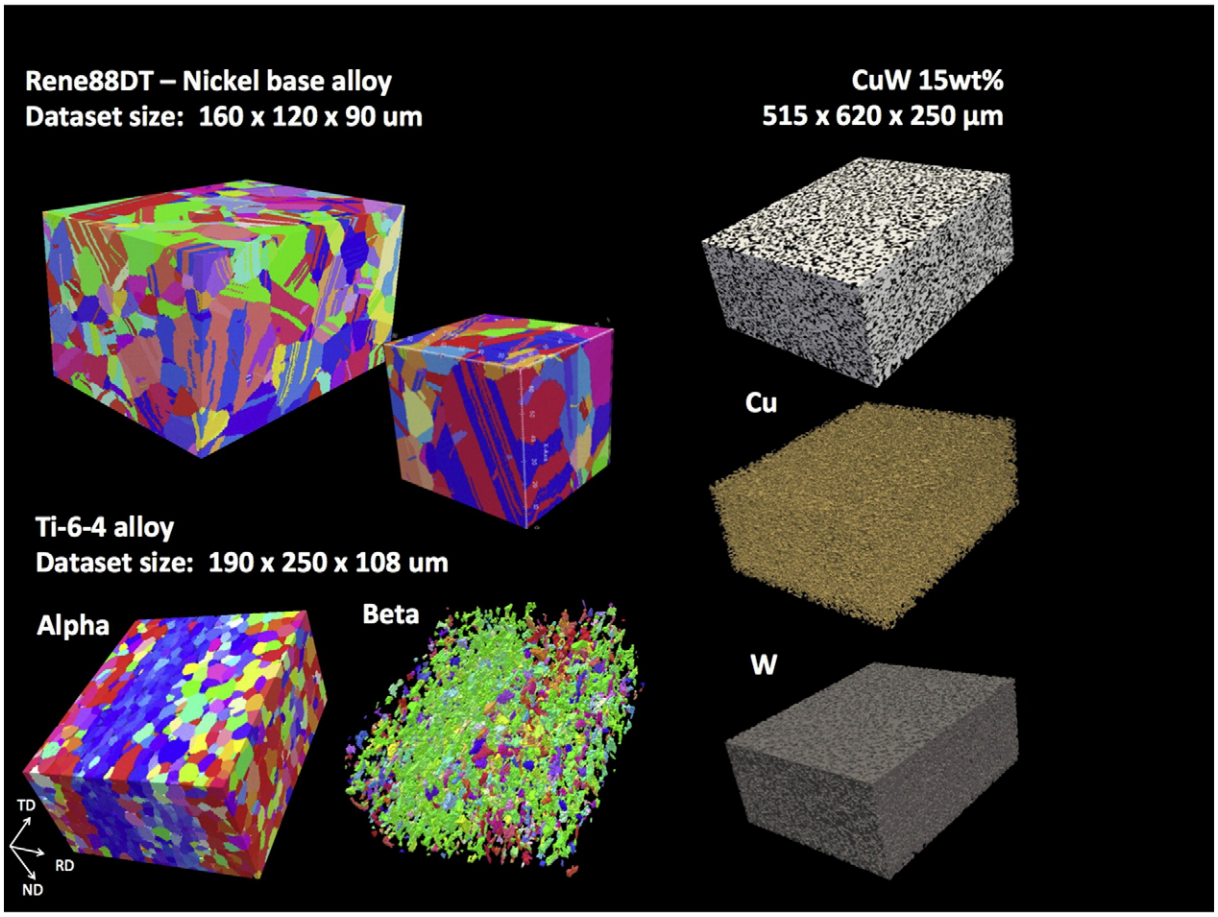

Fig. 11. Examples of reconstructed datasets collected using the TriBeam system, with imaging modalities of EBSD and secondary electron images. In the top left, grain orientation and twin boundary information for a polycrystalline nickel base alloy are collected for use in fatigue life predictions. The bottom left reconstructions show a titanium 6-4 alloy with grain orientations for both alpha and beta phases resolved. The three images on the right show a tungsten copper composite with the phases segmented from secondary electron images, for use in modeling Cu evaporative cooling and fluid flow at high temperatures.

having normal incidence to the beam (shown in Fig. 5b) [25,23] or with the beam parallel to the sample surface (shown in Fig. 5a) [74]. Selection of the slice thickness requires consideration of the resolution of the features of interest in the sample and the size of the dataset to be collected. Slice thicknesses of 250 nm have been demonstrated, but it is believed that a slice resolution of 100 nm should be obtainable by limiting the number of piezo positioner axis movements per iterative cycle. In Fig. 11, reconstructed datasets of W–Cu composites, a Ti-6-4 alloy, and a

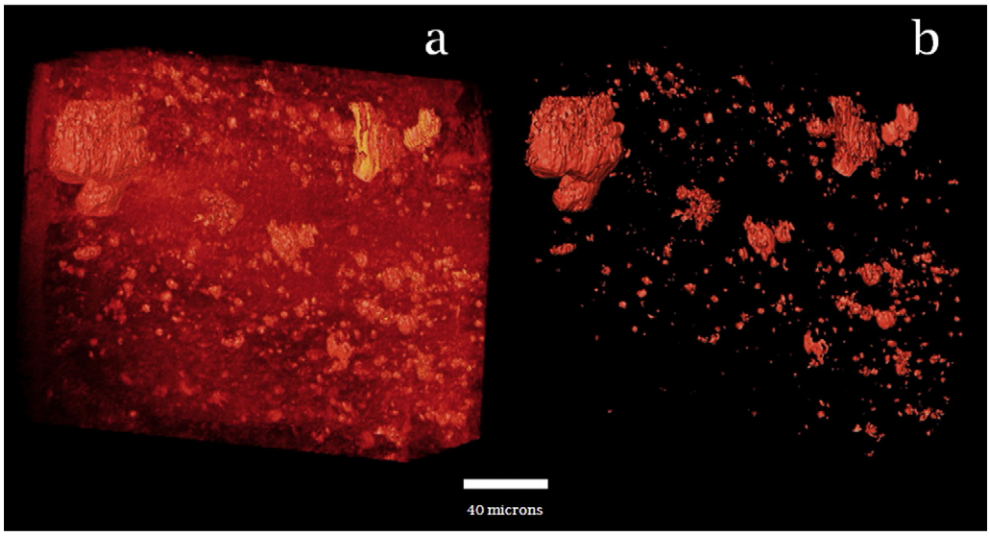

Fig. 12. A three dimensional reconstruction of a 3.6 million µm3 geological sample serially sectioned (200 nm slice thickness) in the TriBeam. Backscattered electron data were collected during an automated 8 hour run. a) shows a high Z material embedded in a mineral matrix. The matrix has been removed in b) to highlight the material of interest.

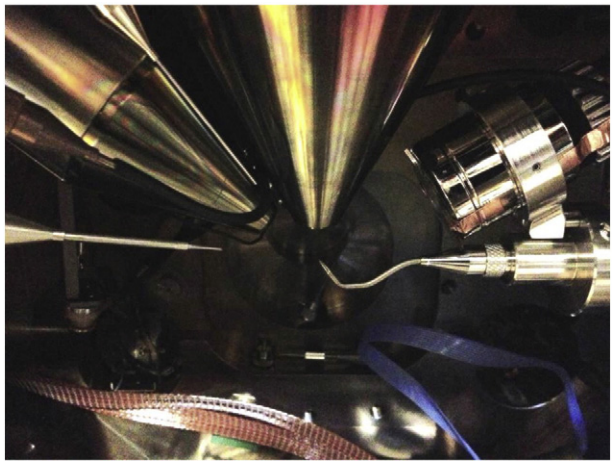

Fig. 13. An image showing the TriBeam gas injection system. The gas flow tube is located directly beneath the microscope objective used to focus the laser light.

nickel base alloy Rene88DT are shown. Both the titanium and nickel datasets are composed of EBSD information at every slice, and the W–Cu alloy dataset is a secondary electron SEM image dataset. The TriBeam has also been used to collect datasets from geological samples which can contain information such as high Z number elements of interest, as shown in Fig. 12. Since the femtosecond laser induces only limited amounts of damage in most materials, shown in Section 2, laser ablated surfaces can be directly imaged using EBSD, EDS, and other in situ SEM detectors without further preparation. Depending on the material being analyzed, EBSD pattern quality and acquisition speed can be improved by subsequently performing high kV, high current, glancing angle Ga^+ ion milling on the sample surface after laser machining.

3.2. Multimodality

The TriBeam system allows for the collection of multiple, spatially correlated, imaging modalities capable of providing chemical, structural, and topographical information. These voxelized coordinated data can be considered simultaneously to help identify microstructures that could not be characterized without multiple data types. This methodology has been pursued experimentally in software/hardware packages such as EDAX ChiScan, chemically assisted EBSD/EDS mapping [75] and mutual information/data fusion segmentation protocols [76,77]. The datasets collected from multiple detectors within a TriBeam system can be combined because of the high positioning resolution of the piezo positioners to which the sample is rigidly affixed. At every imaging step or laser machining operation the encoder values are recorded leaving a digital fingerprint of the actions performed, which can be used to model the sample geometry and potentially feed into forward models for electron imaging and EBSD [78,79].

3.3. Femtosecond laser-induced surface chemistry

Continuous wave (CW) and nanosecond pulse laser-induced surface chemistry for the deposition of metals and dielectrics have been reviewed extensively [80–82]. In general, the dissociation mechanisms that govern laser-induced deposition can be divided into two categories, photolysis and pyrolysis. Photolytically driven deposition involves the dissociation of surface adsorbed or gas-phase precursor molecules by the direct absorption of one or more photons. Energy transferred to the molecule by the photon or photons drives transitions between vibrational, electronic, and/or rotational states of the molecular system. Pyrolytic deposition, by contrast, occurs when the absorption of photons by the substrate leads to a local increase in temperature that ultimately drives the thermal dissociation of nearby adsorbates. As a result, the characteristics of the substrate, gas precursor, laser wavelength, pulse width, and experimental configuration determine which of these processes dominate.

Both photolytic- and pyrolytic-mediated laser-induced depositions driven by CW and nanosecond pulse lasers suffer from poor spatial resolution. The application of UPLs to laser-induced deposition (LID) holds promise for improving spatial resolution, particularly with regard to photolytic processes where ultrashort pulses at the wavelength at which the precursor gas is transparent may be used to drive nonlinear dissociation only in the focal region of the laser beam.

Haight et al. [83] photolytically deposited sub-diffraction limited chromium lines, down to 200 nm, on a variety of substrates via UPL irradiation in gaseous chromium hexacarbonyl ($Cr(CO)_6$) at atmospheric pressure. Zhang et al. [84] deposited tungsten nanogratings with sub-100 nm linewidths and sub-wavelength ($\lambda/2$) periods on sapphire (Al_2O_3) samples irradiated with 150 fs pulses ($\lambda = 400$ nm, rep rate = 80 MHz) in a tungsten hexacarbonyl ($W(CO)_6$) atmosphere. The orientation of the deposited gratings is shown to be parallel to the polarization of the electric field of the laser, with small variations in the morphology possible by varying the scan speed and laser power. As with the work of Haight et al., the negligible absorption of 400 nm laser irradiation in sapphire was cited as evidence that dissociation is

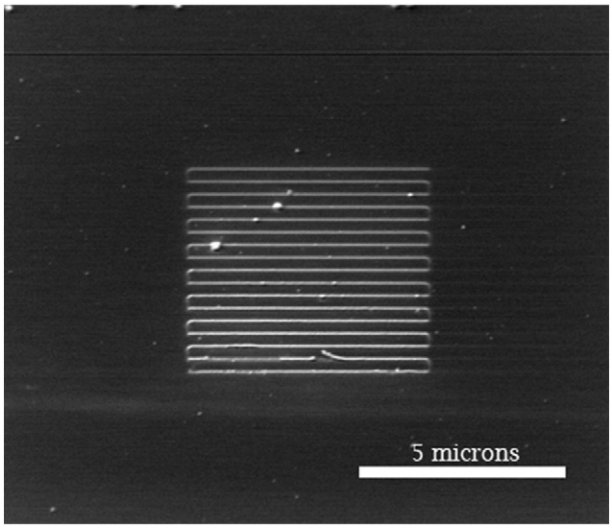

Fig. 14. A SEM image of a serpentine pattern of 60 to 70 nm wide Pt lines deposited via EBID templated laser-induced deposition demonstrating the ability to produce sub-diffraction limited features.

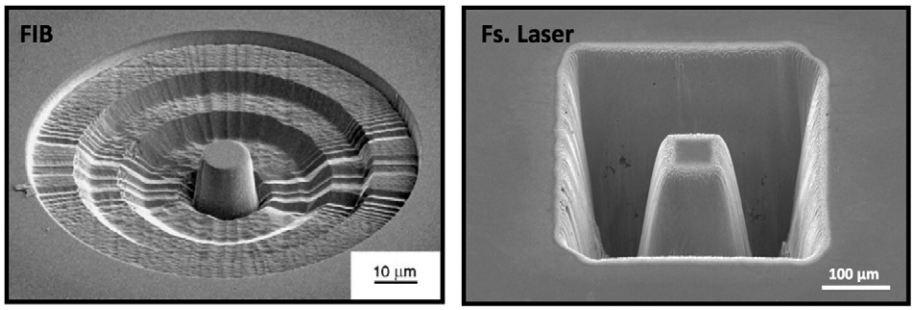

Fig. 15. (Left) A micromachined pedestal created using a FIB which required roughly 4 h to fabricate [93]. (Right) Femtosecond laser micromachining of a volume of 400 μm × 400 μm × 400 μm, which required approximately 3 min of machining time. These structures can then be used for microcompression testing or other types of surface structuring applications.

not due to photoexcited carriers in the substrate, but rather the direct absorption of incident photons.

3.3.1. Electron beam templated fs laser induced deposition

The TriBeam provides an ideal platform for performing controlled laser-induced surface chemistry experiments, using the gas injection configuration illustrated in Fig. 13. In particular, the ability to capture real-time, high resolution images of the sample during deposition enables excellent control of the beam alignment, focus, and fast exploration of parameter space. For instance, the enhancement of both deposition rate and spatial resolution for templated electron beam UPL-induced deposition has been demonstrated [26]. During this process, electron beam-induced deposition (EBID) is used to create a thin, arbitrarily shaped patterned template, which is then illuminated with femtosecond laser pulses while being exposed to a gas precursor of choice. Material initially deposits preferentially on the UPL EBID template at rates 2 to 6 times faster than traditional EBID (depending on the template thickness). In this fashion, features smaller than the diffraction limit of the laser wavelength can be deposited. For example, Fig. 14 shows a serpentine pattern of platinum produced using this technique. The precursor employed in this example was (trimethyl) methylcyclopentadienylplatinum ($Pt(MeCp)Me_3$) and the process yielded lines on the order of 60 to 70 nm wide with a 250 nm pitch — far below the diffraction limit. EBID templates as thin as 10 nm have been shown to be effective nucleation sites for UPL-induced deposition [26].

3.3.2. Plasmon mediated fs laser induced deposition

The TriBeam's efficacy as a tool for exploring the interaction of light and matter has led to the recent demonstration of a novel mechanism of precursor dissociation. Untemplated UPL-induced platinum deposition was demonstrated on gold substrates without laser-induced sample heating (given the reflectivity of gold at 775 nm) using photons having insufficient energy to photolytically dissociate the precursor employed ($Pt(MeCp)Me_3$), indicating a purely plasmonic mechanism for dissociation [26]. Previously, surface plasmon-mediated laser-induced deposition has been reported only in the context of enhancement of photolytic processes [59,85].

The mechanism proposed involves the local enhancement of the electric field at the surface where constructive interference between laser-induced surface plasmons and the laser field occurs. While not sufficient to modify the surface under the conditions used in these experiments, the superposition of fields provides sufficient energy to dissociate the precursor. The coherent periodicity of the deposits and the dependency of its orientation on the orientation of the polarization of incident laser radiation further support a field-mediated mechanism. On substrates with empty conduction bands and large band gaps (dielectrics), the absence of free electrons precludes the existence of surface plasmons. Experimentally, this resulted in the absence of coherence in the morphology of platinum deposited on absorbing dielectrics (black glass). No platinum deposition was observed with this precursor at this wavelength on transparent dielectrics (optical grade SiO_2). In addition, the deposition rate was found to be notably higher on gold, where the plasmon resonance is close to the frequency of the incident laser light, than on platinum, providing further support for a plasmonic dissociation mechanism.

3.4. Micromachining/sample fabrication

Many sample fabrication techniques that are routinely performed in focused ion beam systems can be duplicated using the femtosecond laser. For example, micropillars for micromechanical testing experiments can be fabricated with the femtosecond laser as shown in Fig. 15. Targeted micropillar fabrication can also be performed after identifying features of interest such as specific grain orientations (using EBSD), regions of chemical segregation (EDS), or morphological features (BSE or SE). The rate of material removal with a femtosecond laser is 4–5 orders of magnitude faster than a gallium source FIB, so large arrays of pillars, trenches, or regions of surface texturing can be fabricated in short amounts of time. Devices have already been fabricated ex situ for microfluidic devices [86], gratings [87–89], waveguides [10], and fibers for lab-on-a-chip [90]. These devices can be fabricated in situ via the TriBeam system and immediately characterized or modified on a finer scale in a combined processing route by using the FIB.

4. Future directions

Ultrashort pulse laser systems have been integrated into scanning electron beam microscopes for material removal, beam chemistry, and more broadly material tomography with unprecedented material removal speed and a limited damage zone. In the near future, we expect to see data processing to be performed real-time during data collection, which could lead to electron imaging optimization and intelligent volume sampling approaches. For instance, tomographic sectioning could stop after a sufficient volume of material was collected to characterize a certain set of material properties. It is expected that tabletop single pulse experiments could be replicated in the chamber leading to throughput enhancements for techniques such as laser induced breakdown spectroscopy (LIBS) for chemical analysis, damage threshold studies for laser–material interactions, or delamination experiments. We also anticipate that processing of custom materials will be possible with combination of additive beam chemistry and subtractive laser ablation.

Acknowledgments

The authors acknowledge the Office of Naval Research ONR-DURIP grant #N000141010783 (Julie Christodoulou, David Shifler) for support of the development of the TriBeam system. The authors also thank the FEI Corporation for supporting the development of the TriBeam system. Additionally we thank Remco Geurts (FEI) and Yuri Rikers (FEI) for aiding in work on the WC-Co tomography experiments and Ali Gholinia

(University of Manchester) for providing the samples. We also acknowledge the useful discussions with Steven Yalisove and John Nees during early laser development work. The support of the U.S. Air Force grant FA9550-12-1-0445 and ONR grants N00014-12-1-0039 and N00014-12-1-0075 for tomography development is also gratefully acknowledged.

References

[1] D. Strickland, G. Mourou, Compression of amplified chirped optical pulses, Opt. Commun. 56 (3) (1985) 219–221.
[2] J.B. Jackson, M. Mourou, J.F. Whitaker, I.N. Duling III, S.I. Williamson, M. Menu, G.A. Mourou, Terahertz imaging for non-destructive evaluation of mural paintings, Opt. Commun. 281 (4) (2008) 527–532, http://dx.doi.org/10.1016/j.optcom.2007.10.049.
[3] T. Juhasz, F. Loesel, R. Kurtz, C. Horvath, J. Bille, G. Mourou, Corneal refractive surgery with femtosecond lasers, IEEE J. Sel. Top. Quantum Electron. 5 (4) (1999) 902–910, http://dx.doi.org/10.1109/2944.796309.
[4] B.R. Tull, J.E. Carey, E. Mazur, J.P. McDonald, S.M. Yalisove, Silicon surface morphologies after femtosecond laser irradiation, MRS Bull. 31 (2006) 626–633, http://dx.doi.org/10.1557/mrs2006.160.
[5] C. Rose-Petruck, R. Jimenez, T. Guo, A. Cavalleri, C.W. Siders, F. Rksi, J.A. Squier, B.C. Walker, K.R. Wilson, C.P.J. Barty, Picosecond–milliangstrom lattice dynamics measured by ultrafast X-ray diffraction, Nature 398 (6725) (1999) 310–312, http://dx.doi.org/10.1038/18631.
[6] M. Bargheer, N. Zhavoronkov, Y. Gritsai, J.C. Woo, D.S. Kim, M. Woerner, T. Elsaesser, Coherent atomic motions in a nanostructure studied by femtosecond X-ray diffraction, Science 306 (5702) (2004) 1771–1773, http://dx.doi.org/10.1126/science.1104739.
[7] S. Gupta, J. Whitaker, G. Mourou, Ultrafast carrier dynamics in III–V semiconductors grown by molecular-beam epitaxy at very low substrate temperatures, IEEE J. Quantum Electron. 28 (10) (1992) 2464–2472, http://dx.doi.org/10.1109/3.159553.
[8] Q. Feng, Y. Picard, J. McDonald, P.V. Rompay, S. Yalisove, T. Pollock, Femtosecond laser machining of single-crystal superalloys through thermal barrier coatings, Mater. Sci. Eng. A 430 (1–2) (2006) 203–207, http://dx.doi.org/10.1016/j.msea.2006.05.104.
[9] S. Kyu Kim, S. Pedersen, A.H. Zewail, Femtochemistry of organometallics: dynamics of metal–metal and metal–ligand bond cleavage in $M_2(CO)_{10}$, Chem. Phys. Lett. 233 (1995) 500–508, http://dx.doi.org/10.1016/0009-2614(95)00050-E.
[10] R.R. Gattass, E. Mazur, Femtosecond laser micromachining in transparent materials, Nat. Photon. 2 (4) (2008) 219–225, http://dx.doi.org/10.1038/nphoton.2008.47.
[11] X. Liu, D. Du, G. Mourou, Laser ablation and micromachining with ultrashort laser pulses, IEEE J. Quantum Electron. 33 (10) (1997) 1706–1716, http://dx.doi.org/10.1109/3.631270.
[12] Q. Feng, Y. Picard, H. Liu, S. Yalisove, G. Mourou, T. Pollock, Femtosecond laser micromachining of a single-crystal superalloy, Scr. Mater. 53 (5) (2005) 511–516, http://dx.doi.org/10.1016/j.scriptamat.2005.05.006.
[13] S. Ma, J.P. McDonald, B. Tryon, S.M. Yalisove, T.M. Pollock, Femtosecond laser ablation regimes in a single-crystal superalloy, Metall. Mater. Trans. A 38 (13) (2007) 2349–2357, http://dx.doi.org/10.1007/s11661-007-9260-0.
[14] Y.N. Picard, D.P. Adams, J.A. Palmer, S.M. Yalisove, Pulsed laser ignition of reactive multilayer films, Appl. Phys. Lett. 88 (14) (2006), http://dx.doi.org/10.1063/1.2191952.
[15] Y.N. Picard, S.M. Yalisove, Femtosecond laser heat affected zones profiled in cosi multilayer thin films, Appl. Phys. 92 (1) (2008), http://dx.doi.org/10.1063/1.2832640.
[16] J.P. McDonald, D.K. Das, J.A. Nees, T.M. Pollock, S.M. Yalisove, Approaching non-destructive surface chemical analysis of CMSX-4 superalloy with double-pulsed laser induced breakdown spectroscopy, Spectrochim. Acta B At. Spectrosc. 63 (5) (2008) 561–565, http://dx.doi.org/10.1016/j.sab.2008.02.004.
[17] D. Das, J. McDonald, S. Yalisove, T. Pollock, Depth-profiling study of a thermal barrier coated superalloy using femtosecond laser-induced breakdown spectroscopy, Spectrochim. Acta B At. Spectrosc. 63 (1) (2008) 27–36, http://dx.doi.org/10.1016/j.sab.2007.10.048.
[18] D.K. Das, J.P. McDonald, C.G. Levi, S.M. Yalisove, T.M. Pollock, Detection of a marker layer in a 7YSZ thermal barrier coating by femtosecond laser-induced breakdown spectroscopy, Surf. Coat. Technol. 202 (16) (2008) 3940–3946, http://dx.doi.org/10.1016/j.surfcoat.2008.02.003.
[19] D.K. Das, T.M. Pollock, Femtosecond laser machining of cooling holes in thermal barrier coated CMSX4 superalloy, J. Mater. Process. Technol. 209 (15–16) (2009) 5661–5668, http://dx.doi.org/10.1016/j.jmatprotec.2009.05.031.
[20] C.-C. Chen, D.-J. Lee, T. Pollock, J.F. Whitaker, Pulsed-terahertz reflectometry for health monitoring of ceramic thermal barrier coatings, Opt. Express 18 (4) (2010) 3477–3486, http://dx.doi.org/10.1364/OE.18.003477.
[21] B. Hou, J. Easter, K. Krushelnick, J.A. Nees, Generation of hard X-rays by femtosecond laser pulse interaction with Cu in laminar helium flow in ambient air, Appl. Phys. Lett. 92 (16) (2008), http://dx.doi.org/10.1063/1.2917442 (161501-161501-3).
[22] K.-H. Liao, A.G. Mordovanakis, B. Hou, G. Chang, M. Rever, G.A. Mourou, J. Nees, A. Galvanauskas, Generation of hard X-rays using an ultrafast fiber laser system, Opt. Express 15 (21) (2007) 13942–13948, http://dx.doi.org/10.1364/OE.15.013942.
[23] M.P. Echlin, N.S. Husseini, J.A. Nees, T.M. Pollock, A new femtosecond laser-based tomography technique for multiphase materials, Adv. Mater. 23 (20) (2011) 2339–2342, http://dx.doi.org/10.1002/adma.201003600.
[24] M.P. Echlin, T.M. Pollock, A statistical sampling approach for measurement of fracture toughness parameters in a 4330 steel by 3-d femtosecond laser-based tomography, Acta Mater. 61 (15) (2013) 5791–5799, http://dx.doi.org/10.1016/j.actamat.2013.06.023.
[25] M.P. Echlin, A. Mottura, C. Torbet, T.M. Pollock, A new TriBeam system for three-dimensional multimodal analysis, Rev. Sci. Instrum. 83 (2) (2012) 023701, http://dx.doi.org/10.1063/1.3680111.
[26] M. Straw, Ultrashort pulsed laser-induced chemistry: methodology, instrumentation, and analysisPh.D. thesis University of Technology, Sydney, 2013.
[27] M. Straw, S. Randolph, Direct spatiotemporal analysis of femtosecond laser-induced plasma-mediated chemical reactions, Laser Phys. Lett. 11 (3) (2014) 035601, http://dx.doi.org/10.1088/1612-2011/11/3/035601.
[28] D. Du, X. Liu, G. Korn, J. Squier, G. Mourou, Laser-induced breakdown by impact ionization in SiO_2 with pulse widths from 7 ns to 150 fs, Appl. Phys. Lett. 64 (23) (1994) 3071–3073, http://dx.doi.org/10.1063/1.111350.
[29] C.B. Schaffer, A. Brodeur, E. Mazur, Laser-induced breakdown and damage in bulk transparent materials induced by tightly focused femtosecond laser pulses, Meas. Sci. Technol. 12 (11) (2001) 1784, http://dx.doi.org/10.1088/0957-0233/12/11/305.
[30] B.C. Stuart, M.D. Feit, S. Herman, A.M. Rubenchik, B.W. Shore, M.D. Perry, Nanosecond-to-femtosecond laser-induced breakdown in dielectrics, Phys. Rev. B 53 (1996) 1749–1761, http://dx.doi.org/10.1103/PhysRevB.53.1749.
[31] J.P. Colombier, P. Combis, F. Bonneau, R. Le Harzic, E. Audouard, Hydrodynamic simulations of metal ablation by femtosecond laser irradiation, Phys. Rev. B 71 (2005) 165406, http://dx.doi.org/10.1103/PhysRevB.71.165406.
[32] B.N. Chichkov, C. Momma, S. Nolte, F. Alvensleben, A. Tünnermann, Femtosecond, picosecond and nanosecond laser ablation of solids, Appl. Phys. A 63 (2) (1996) 109–115, http://dx.doi.org/10.1007/BF01567637.
[33] B.J. Demaske, V.V. Zhakhovsky, N.A. Inogamov, I.I. Oleynik, Ablation and spallation of gold films irradiated by ultrashort laser pulses, Phys. Rev. B 82 (2010) 064113, http://dx.doi.org/10.1103/PhysRevB.82.064113.
[34] M. Iyer, V. Gavini, T.M. Pollock, Energetics and nucleation of point defects in aluminum under extreme tensile hydrostatic stresses, Phys. Rev. B 89 (1) (2014), http://dx.doi.org/10.1103/PhysRevB.89.014108.
[35] C. Reina, J. Marian, M. Ortiz, Nanovoid nucleation by vacancy aggregation and vacancy-cluster coarsening in high-purity metallic single crystals, Phys. Rev. B 84 (2011) 104117, http://dx.doi.org/10.1103/PhysRevB.84.104117.
[36] N. Zhang, X. Zhu, J. Yang, X. Wang, M. Wang, Phys. Rev. Lett. 99 (2007) 167602, http://dx.doi.org/10.1103/PhysRevLett.99.167602.
[37] X. Zeng, X.L. Mao, R. Greif, R.E. Russo, Experimental investigation of ablation efficiency and plasma expansion during femtosecond and nanosecond laser ablation of silicon, Appl. Phys. A 80 (2) (2005) 237–241, http://dx.doi.org/10.1007/s00339-004-2963-9.
[38] J.P. McDonald, S. Ma, T.M. Pollock, S.M. Yalisove, J.A. Nees, Femtosecond pulsed laser ablation dynamics and ablation morphology of nickel based superalloy CMSX-4, J. Appl. Phys. 103 (9) (2008), http://dx.doi.org/10.1063/1.2917418.
[39] J. McDonald, Near threshold femtosecond laser interactions with materials: ablation thresholds, morphologies, and dynamicsPh.D. thesis University of Michigan, 2007.
[40] R. Le Harzic, N. Huot, E. Audouard, C. Jonin, P. Laporte, S. Valette, A. Fraczkiewicz, R. Fortunier, Comparison of heat-affected zones due to nanosecond and femtosecond laser pulses using transmission electronic microscopy, Appl. Phys. Lett. 80 (2002) 3886–3888, http://dx.doi.org/10.1063/1.1481195.
[41] A. Kumar, T. Pollock, Mapping of femtosecond laser-induced collateral damage by electron backscatter diffraction, J. Appl. Phys. 110 (8) (2011) 083114, http://dx.doi.org/10.1063/1.3653839.
[42] F. Altmann, J. Beyersdorfer, J. Schischka, M. Krause, G. Franz, L. Kwakman, Cross section analysis of cu filled TSVs based on high throughput plasma-fib milling, Istfa 2012: Conference Proceedings from the 38th International Symposium for Testing and Failure Analysis, vol. 1, ASM International, 2012, p. 39.
[43] M.M. Taklo, A. Klumpp, P. Ramm, L. Kwakman, G. Franz, Bonding and TSV in 3D IC integration: physical analysis with plasma FIB, Microsc. Anal. (2011) 10.
[44] S. Nolte, C. Momma, H. Jacobs, A. Tünnermann, B.N. Chichkov, B. Wellegehausen, H. Welling, Ablation of metals by ultrashort laser pulses, J. Opt. Soc. Am. B 14 (10) (1997) 2716–2722, http://dx.doi.org/10.1364/JOSAB.14.002716.
[45] K. Furusawa, K. Takahashi, H. Kumagai, K. Midorikawa, M. Obara, Ablation characteristics of Au, Ag, and Cu metals using a femtosecond Ti:sapphire laser, Appl. Phys. A 69 (1) (1999) S359–S366, http://dx.doi.org/10.1007/s003390051417.
[46] P. Moreno, C. Méndez, A. García, I. Arias, L. Roso, Femtosecond laser ablation of carbon reinforced polymers, Appl. Surf. Sci. 252 (12) (2006) 4110–4119, http://dx.doi.org/10.1016/j.apsusc.2005.06.008.
[47] S. Valette, P. Steyer, L. Richard, B. Forest, C. Donnet, E. Audouard, Influence of femtosecond laser marking on the corrosion resistance of stainless steels, Appl. Surf. Sci. 252 (13) (2006) 4696–4701, http://dx.doi.org/10.1016/j.apsusc.2005.07.16.
[48] J. Koch, E. Fadeeva, M. Engelbrecht, C. Ruffert, H. Gatzen, A. Ostendorf, B. Chichkov, Maskless nonlinear lithography with femtosecond laser pulses, Appl. Phys. A 82 (1) (2006) 23–26, http://dx.doi.org/10.1007/s00339-005-3418-7.
[49] J.E. Sipe, J.F. Young, J.S. Preston, H.M. Van Driel, Laser-induced periodic surface structure. I. Theory, Phys. Rev. B 27 (2) (1983) 1141–1154, http://dx.doi.org/10.1103/PhysRevB.27.1141.
[50] J.F. Young, J.S. Preston, H.M. Van Driel, J.E. Sipe, Laser-induced periodic surface structure. II. Experiments on Ge, Si, Al, and brass, Phys. Rev. B 27 (2) (1983) 1155–1172, http://dx.doi.org/10.1103/PhysRevB.27.1155.
[51] Q. Wu, Y. Ma, R. Fang, Y. Liao, Q. Yu, X. Chen, K. Wang, Femtosecond laser-induced periodic surface structure on diamond film, Appl. Phys. Lett. 82 (11) (2003) 1703–1705, http://dx.doi.org/10.1063/1.1561581.
[52] A. Borowiec, H.K. Haugen, Subwavelength ripple formation on the surfaces of compound semiconductors irradiated with femtosecond laser pulses, Appl. Phys. Lett. 82 (25) (2003) 4462–4464, http://dx.doi.org/10.1063/1.1561581.

[53] Y. Shimotsuma, P.G. Kazansky, J. Qiu, K. Hirao, Self-organized nanogratings in glass irradiated by ultrashort light pulses, Phys. Rev. Lett. 91 (24) (2003) 247405/1–247405/4, http://dx.doi.org/10.1103/PhysRevLett.91.247405.
[54] M.Munz J. Bonse H. Sturm, Structure formation on the surface of indium phosphide irradiated by femtosecond laser pulses, J. Appl. Phys. 97 (1) (2005), http://dx.doi.org/10.1063/1.1827919.
[55] O. Varlamova, F. Costache, M. Ratzke, J. Reif, Control parameters in pattern formation upon femtosecond laser ablation, Appl. Surf. Sci. 253 (19) (2007) 7932–7936, http://dx.doi.org/10.1016/j.apsusc.2007.02.067.
[56] V.S.Makin A. Y. Vorobyev C. Guo, Periodic ordering of random surface nanostructures induced by femtosecond laser pulses on metals, J. Appl. Phys. 101 (3) (2007), http://dx.doi.org/10.1063/1.2432288.
[57] A.Rosenfeld J. Bonse J. KrÃüger, On the role of surface plasmon polaritons in the formation of laser-induced periodic surface structures upon irradiation of silicon by femtosecond-laser pulses, J. Appl. Phys. 106 (10) (2009), http://dx.doi.org/10.1063/1.3261734.
[58] M. Huang, F. Zhao, Y. Cheng, N. Xu, Z. Xu, Origin of laser-induced near-subwavelength ripples: interference between surface plasmons and incident laser, ACS Nano 3 (12) (2009) 4062–4070.
[59] S.R.J. Brueck, D.J. Ehrlich, Stimulated surface-plasma-wave scattering and growth of a periodic structure in laser-photodeposited metal films, Phys. Rev. Lett. 48 (24) (1982) 1678–1681.
[60] L. Giannuzzi, F. Stevie, Introduction to Focused Ion Beams: Instrumentation, Theory, Techniques and Practice, Springer, 2005. (URL http://books.google.com/books?id=h1sM6iwg4-wC).
[61] T. Ishitani, T. Yaguchi, Cross-sectional sample preparation by focused ion beam: a review of ion-sample interaction, Microsc. Res. Tech. 35 (4) (1996) 320–333, http://dx.doi.org/10.1002/(SICI)1097-0029(19961101)35:4<320::AID-JEMT3>3.0.CO;2-Q.
[62] M.D. Uchic, L. Holzer, B.J. Inkson, E.L. Principe, P. Munroe, Three-dimensional microstructural characterization using focused ion beam tomography, MRS Bull. 32 (2007) 408–416, http://dx.doi.org/10.1557/mrs2007.64 (URL http://journals.cambridge.org/article_S0883769400007284).
[63] P. Munroe, The application of focused ion beam microscopy in the material sciences, Mater. Charact. 60 (1) (2009) 2–13, http://dx.doi.org/10.1016/j.matchar.2008.11.014 (URL http://www.sciencedirect.com/science/article/pii/S1044580308003306).
[64] T. Gorelik, M. Will, S. Nolte, A. Tuennermann, U. Glatzel, Transmission electron microscopy studies of femtosecond laser induced modifications in quartz, Appl. Phys. A 76 (3) (2003) 309–311, http://dx.doi.org/10.1007/s00339-002-1813-x.
[65] A. Borowiec, M. MacKenzie, G. Weatherly, H. Haugen, Transmission and scanning electron microscopy studies of single femtosecond-laser-pulse ablation of silicon, Appl. Phys. A Mater. Sci. Process. 76 (2) (2003) 201–207, http://dx.doi.org/10.1007/s003390201409.
[66] T.H.R. Crawford, J. Yamanaka, G.A. Botton, H.K. Haugen, High-resolution observations of an amorphous layer and subsurface damage formed by femtosecond laser irradiation of silicon, J. Appl. Phys. 103 (5) (2008), http://dx.doi.org/10.1063/1.2885111.
[67] A. Borowiec, M. MacKenzie, G.C. Weatherly, H.K. Haugen, Femtosecond laser pulse ablation of GaAs and InP: studies utilizing scanning and transmission electron microscopy, Appl. Phys. A 77 (3-4) (2003) 411–417, http://dx.doi.org/10.1007/s00339-002-1949-8.
[68] S. Rubanov, P.R. Munroe, FIB-induced damage in silicon, J. Microsc. 214 (3) (2004) 213–221, http://dx.doi.org/10.1111/j.0022-2720.2004.01327.x.
[69] Y. Dikmelik, C. McEnnis, J.B. Spicer, Femtosecond-laser-induced breakdown spectroscopy of explosives, Proc. SPIE 6217 (2006), http://dx.doi.org/10.1117/12.672886 (62172A-62172A-9).
[70] Y. Dikmelik, C. McEnnis, J.B. Spicer, Femtosecond and nanosecond laser-induced breakdown spectroscopy of trinitrotoluene, Opt. Express 16 (8) (2008) 5332–5337, http://dx.doi.org/10.1364/OE.16.005332.
[71] I. Cravetchi, M. Taschuk, Y. Tsui, R. Fedosejevs, Evaluation of femtosecond libs for spectrochemical microanalysis of aluminium alloys, Anal. Bioanal. Chem. 385 (2) (2006) 287–294, http://dx.doi.org/10.1007/s00216-005-0287-z.
[72] R.W. Schoenlein, W.Z. Lin, J.G. Fujimoto, G.L. Eesley, Femtosecond studies of nonequilibrium electronic processes in metals, Phys. Rev. Lett. 58 (1987) 1680–1683, http://dx.doi.org/10.1103/PhysRevLett.58.1680.
[73] A.J. Sabbah, D.M. Riffe, Femtosecond pump-probe reflectivity study of silicon carrier dynamics, Phys. Rev. B 66 (2002) 165217, http://dx.doi.org/10.1103/PhysRevB.66.165217.
[74] M. Echlin, A. Mottura, M. Wang, P. Mignone, D. Riley, G. Franks, T. Pollock, Three-dimensional characterization of the permeability of W-–Cu composites using a new "TriBeam" technique, Acta MaterActa Mater. 64 (5) (2013) 307–315, http://dx.doi.org/10.1016/j.actamat.2013.10.043.
[75] M.M. Nowell, S.I. Wright, Phase differentiation via combined EBSD and XEDS, J. Microsc. 213 (3) (2004) 296–305, http://dx.doi.org/10.1111/j.0022-2720.2004.01299.x.
[76] J. MacSleyne, M. Uchic, J. Simmons, M.D. Graef, Three-dimensional analysis of secondary γ′ precipitates in René-88 DT and UMF-20 superalloys, Acta Mater. 57 (20) (2009) 6251–6267, http://dx.doi.org/10.1016/j.actamat.2009.08.053.
[77] E. Gulsoy, J. Simmons, M.D. Graef, Application of joint histogram and mutual information to registration and data fusion problems in serial sectioning microstructure studies, Scr. Mater. 60 (6) (2009) 381–384, http://dx.doi.org/10.1016/j.scriptamat.2008.11.004.
[78] A. Winkelmann, Dynamical effects of anisotropic inelastic scattering in electron backscatter diffraction, Ultramicroscopy 108 (12) (2008) 1546–1550, http://dx.doi.org/10.1016/j.ultramic.2008.05.002.
[79] P.G. Callahan, M. De Graef, Dynamical electron backscatter diffraction patterns. Part I: pattern simulations, Microsc. Microanal. 19 (2013) 1255–1265, http://dx.doi.org/10.1017/S1431927613001840.
[80] Y. Rytz-Froidevaux, R.P. Salathe, H.H. Gilgen, Laser generated microstructures, Appl. Phys. A Solids Surf. 37 (3) (1985) 121–138.
[81] F.A. Houle, Basic mechanisms in laser etching and deposition, Appl. Phys. A Mater. Sci. Process. 41 (4) (1986) 315–330.
[82] I.P. Herman, Laser-assisted deposition of thin films from gas-phase and surface-adsorbed molecules, Chem. Rev. 89 (6) (1989) 1323–1357.
[83] R. Haight, P. Longo, A. Wagner, Metal deposition with femtosecond light pulses at atmospheric pressure, J. Vac. Sci. Technol. A Vacuum, Surf. Films 21 (3) (2003) 649–652.
[84] H. Zhang, M. Tang, J. McCoy, T.H. Her, Deposition of tungsten nanogratings induced by a single femtosecond laser beam, Opt. Express 15 (10) (2007) 5937–5947.
[85] C.J. Chen, R.M. Osgood, Direct observation of the local-field-enhanced surface photochemical reactions, Phys. Rev. Lett. 50 (21) (1983) 1705–1708.
[86] J.P. McDonald, V.R. Mistry, K.E. Ray, S.M. Yalisove, Femtosecond pulsed laser direct write production of nano- and microfluidic channels, Appl. Phys. Lett. 88 (18) (2006), http://dx.doi.org/10.1063/1.2201620.
[87] A. Martinez, M. Dubov, I. Khrushchev, I. Bennion, Direct writing of fibre Bragg gratings by femtosecond laser, Electron. Lett. 40 (19) (2004) 1170–1172, http://dx.doi.org/10.1049/el:20046050.
[88] Y. Kondo, K. Nouchi, T. Mitsuyu, M. Watanabe, P.G. Kazansky, K. Hirao, Fabrication of long-period fiber gratings by focused irradiation of infrared femtosecond laser pulses, Opt. Lett. 24 (10) (1999) 646–648, http://dx.doi.org/10.1364/OL.24.000646.
[89] P.P. Pronko, S.K. Dutta, J. Squier, J.V. Rudd, D. Du, G. Mourou, Machining of sub-micron holes using a femtosecond laser at 800 nm, Opt. Commun. 114 (1-2) (1995) 106–110, http://dx.doi.org/10.1016/0030-4018(94)00585-I.
[90] Y. Cheng, K. Sugioka, K. Midorikawa, Freestanding optical fibers fabricated in a glass chip using femtosecond laser micromachining for lab-on-a-chip application, Opt. Express 13 (18) (2005) 7225–7232.
[91] S.K. Sundaram, E. Mazur, Inducing and probing non-thermal transitions in semiconductors using femtosecond laser pulses, Nat. Mater. 1 (4) (2002) 217–224.
[92] M. Echlin, A new femtosecond laser-based 3D tomography technique, Ph.D. thesis University of Michigan, 2011.
[93] M.D. Uchic, D.M. Dimiduk, A methodology to investigate size scale effects in crystalline plasticity using uniaxial compression testing, Mater. Sci. Eng. A 400–401 (0) (2005) 268–278, http://dx.doi.org/10.1016/j.msea.2005.03.082.